Available online at www.sciencedirect.com
ScienceDirect
Applied Acoustics 68 (2007) 217–237
applied acoustics
www.elsevier.com/locate/apacoust

Three-dimensional linearised Euler model simulations of sound propagation in idealised urban situations with wind effects

Dietrich Heimann

DLR Institute of Atmospheric Physics, Oberpfaffenhofen, 82234 Wessling, Germany

Revised 30 May 2005; accepted 3 October 2005
Available online 28 November 2005

Abstract

A three-dimensional numerical time-domain model based on the linearised Euler equation is applied to idealised urban situations with elongated, isolated buildings beside a straight street with sound emissions. The paper aims at the investigation of principle relationships between the source–receiver geometry (street and building facades) and sound propagation under the consideration of ground and wind. By applying cyclic lateral boundary conditions for either one or both horizontal co-ordinates, two different idealised urban environments were considered: a single street and parallel streets. Numerical experiments were performed to elaborate the effects of different roof types, ground properties, wind flow, and turbulence in both urban environments with the focus on the back facades ('quiet' sides) of the buildings. As a result it was found that the back facades of flat-roof buildings are quieter than those of hip roof buildings despite equal cross-cut areas. The wind effect (resulting in quieter upwind and louder downwind facades) is more pronounced for hip-roof buildings. In the case of parallel streets upwind facades are slightly louder than downwind facades because they are simultaneously exposed to downwind propagating sound from the next parallel street.

Keywords: Propagation; Linear Euler model; Buildings; Wind; Turbulence

1. Introduction

Noise from traffic or industrial sources causes nuisances in urban areas since a long time (e.g. [5]). The problem is enhanced by the coincidence of a high population density, an

E-mail address: d.heimann@dlr.de

0003-682X/$ - see front matter © 2005 Elsevier Ltd. All rights reserved.
doi:10.1016/j.apacoust.2005.10.002

intense and often still growing traffic volume, short distances between source and receiver, and multiple reflections in street canyons. Nowadays, the reduction of noise in cities and the creation of quiet areas is more and more in the focus of urban planning and traffic management. The development and implementation of effective and efficient measures requires specialised noise propagation models which take into account the relevant processes of noise propagation in complex urban environments.

A variety of computational approaches for the prediction of noise in cities was published in the past. Most models presently used in practice are based on the superposition of direct and reflected sound rays [6]. Heutschi [8] proposed the use of look-up tables that were generated by numerous ray tracing calculations for standardised geometries of buildings along a straight street. Other authors discuss specific variants of ray models (e.g. [9,14,15,20]). An extension of the ray based methods is the introduction of sound particles with statistical behaviour. These methods account for random scattering and diffusion of the sound energy (e.g. [12,13]). A further type of models considers the propagation of sound between buildings as a diffusion process and solves numerically the diffusion equation (e.g. [16,17]). Also radiosity-based models, originally developed to assess heat transfer or illumination, were applied to urban sound propagation [10,11]. Recently, a finite-difference time-domain sound propagation model was applied to an urban street canyon [19]. In contrast to the aforementioned models, this approach is also capable of considering the influence of temperature stratification, complex air flow and even turbulence in the air. The finite-difference time-domain method is based on the numerical solution of the Euler equation. It enables the simulation of sound propagation without limitations with respect to the geometrical shape of obstacles [3,4]. Moreover, it is capable of considering complex meteorological situations [1,2] and ground effects [18]. A major shortcoming is its rather high run time consumption and memory requirement, in particular if high frequencies are involved. Therefore, applications of this type of model are mostly restricted to two dimensions, short ranges, and/or low frequencies.

Also this study is based on a finite-difference time-domain model which numerically solves the linearised Euler equation (referred to as LE model in the following). In contrast to the studies of Van Renterghem [19] who applied the model to a two-dimensional vertical cross-section, the model is used here in full three dimensions. The three-dimensionality allows the consideration of isolated buildings of finite length with wind blowing over and around the buildings. It also accounts for sound diffraction at arbitrarily oriented edges of the buildings.

The purpose of this paper is to show the acoustical shading by elongated building of finite length at both sides of a city street. Numerical experiments were performed to study the influence of two different roof shapes (flat and hip), the effect of wind and turbulence, and the consequence of two different lateral boundary conditions (absorbing or cyclic). The following sections of this paper present the model (Section 2), explain the geometrical set-up of the considered idealised urban situation (Section 3), and describe the experimental layout of the study (Section 4). The results are discussed in Section 5. Eventually, conclusions are drawn in Section 6.

2. The linearized Euler (LE) model

The numerical sound propagation model is defined in an orthogonal co-ordinate system with the horizontal co-ordinates x, y and the vertical co-ordinate z. In the following it is

assumed that any three-dimensional motion $\mathbf{U}$ in the atmosphere is composed of a mean 3D wind vector $\overline{\mathbf{U}}$, a turbulent deviation from the mean wind $\mathbf{U}'$, and a particle velocity $\mathbf{U}''$ superimposed according to acoustical waves:

$$\mathbf{U} = \overline{\mathbf{U}} + \mathbf{U}' + \mathbf{U}''. \tag{1}$$

The mean wind and the turbulent motion can be combined to the meteorological air motion $\mathbf{U}_{\text{met}} = \overline{\mathbf{U}} + \mathbf{U}'$. Analogously, other variables are defined such as the pressure

$$p = \bar{p} + p' + p'' = p_{\text{met}} + p'' \tag{2}$$

with the mean air pressure $\bar{p}$, the turbulent pressure fluctuation p', and the sound pressure p''.

The LE model is based on the equations for adiabatic processes in a friction-less, non-rotating, non-buoyant atmosphere. These equations are linearised with respect to the meteorological background as defined by the wind $\mathbf{U}_{\text{met}}$ and the sound speed $c = (\kappa p_{\text{met}} \rho_{\text{met}}^{-1})^{0.5}$, with the air pressure p_{met}, the air density ρ_{met}, and the ratio of the specific heat capacities at constant pressure and constant volume $\kappa = c_{\text{p}}/c_{\text{v}} = 1.4$.

Provided the meteorological wind is non-divergent ($\nabla \cdot \mathbf{U}_{\text{met}} = 0$) the prognostic (time-domain) equations of the particle velocity and the sound pressure read

$$\frac{\partial \mathbf{U}''}{\partial t} = -(\mathbf{U}_{\text{met}} \cdot \nabla)\mathbf{U}'' - (\mathbf{U}'' \cdot \nabla)\mathbf{U}_{\text{met}} - \alpha_{\text{met}} \nabla p'' - 0.05 R \mathbf{U}'', \tag{3a}$$

$$\frac{\partial p''}{\partial t} = -\mathbf{U}_{\text{met}} \nabla p'' - \kappa p_{\text{met}} \nabla \cdot \mathbf{U}''. \tag{3b}$$

The complete derivation of the model equations is given by Blumrich and Heimann (2002). Even though an absorbing impedance condition is employed at the lateral and upper boundaries of the model domain (Blumrich and Heimann, 2002), a damping term (last term in Eq. (3a)) was introduced to reduce remaining non-physical reflections which mainly appear in the presence of wind. The parameter R is set to zero in the core of the grid volume. The outer parts of the grid volume are used as damping zones where R is calculated as $R = 1 - \sin(0.5\pi d/d_0)$ within a distance $0 \leqslant d \leqslant d_0$ from the respective boundaries. Tests have shown that the depth d_0 of the damping zones should be at least the quadruple of the maximum wave length.

In porous ground modified equations are used according to Salomons et al. [18]:

$$\frac{\partial \mathbf{U}''}{\partial t} = -\frac{\Omega}{c_{\text{s}}} \alpha_{\text{met}} \nabla p'' - \sigma \frac{\Omega}{c_{\text{s}}} \alpha_{\text{met}} \mathbf{U}'' - 0.05 R \mathbf{U}'', \tag{4a}$$

$$\frac{\partial p''}{\partial t} = -\frac{\kappa p_{\text{met}}}{\Omega} \nabla \cdot \mathbf{U}'' \tag{4b}$$

with the effective flow resistivity σ, the effective porosity Ω, and the structure constant of the porous ground c_{s}. In the case of rigid ground, $\mathbf{U}''$ and p'' are set to zero in the ground layer.

Eqs. (3a)/(3b) (in the air) and (4a)/(4b) (in the ground) are numerically integrated in time on an orthogonal staggered grid using first-order forward-in-time, centred-in-space finite differences. Reflecting obstacles like buildings are considered by setting the perpendicular components of the particle velocity to zero at the side walls of the obstacle grid cells. Any three-dimensional non-divergent meteorological wind field $\mathbf{U}_{\text{met}}(x, y, z)$, pressure field $p_{\text{met}}(x, y, z)$, and density field $\rho_{\text{met}}(x, y, z)$ can be used as background.

3. Model domain and topography

In this study the three-dimensional version of the LE model is applied to an idealised urban situation with a straight street parallel to the y-axis and two 34 m long and 8 m wide buildings on either side of the street (Fig. 1). Two different roof types (flat roof and hip roof) were considered. The building heights (8 m for flat-roof buildings, 10 m for hip-roof buildings with 45° roof inclination) were chosen such that all buildings have the same cross-cut area (64 m^2) in the x–z-plane. The volume of the buildings deviates by approx. 3% (flat roof: 2176 m^3, hip roof: 2112 m^3). Sound is emitted from an assumed coherent line source which is located 0.50 m above the surface along the centre line of the street.

The available computer storage capacity enables about $N = 25 \times 10^6$grid cells. Consequently, a numerical model domain is feasible which expands over $L_x = L_y = 46$ m in the horizontal directions ($n_x = n_y = 368$ grid intervals of $\Delta x = \Delta y = 0.125$ m), and

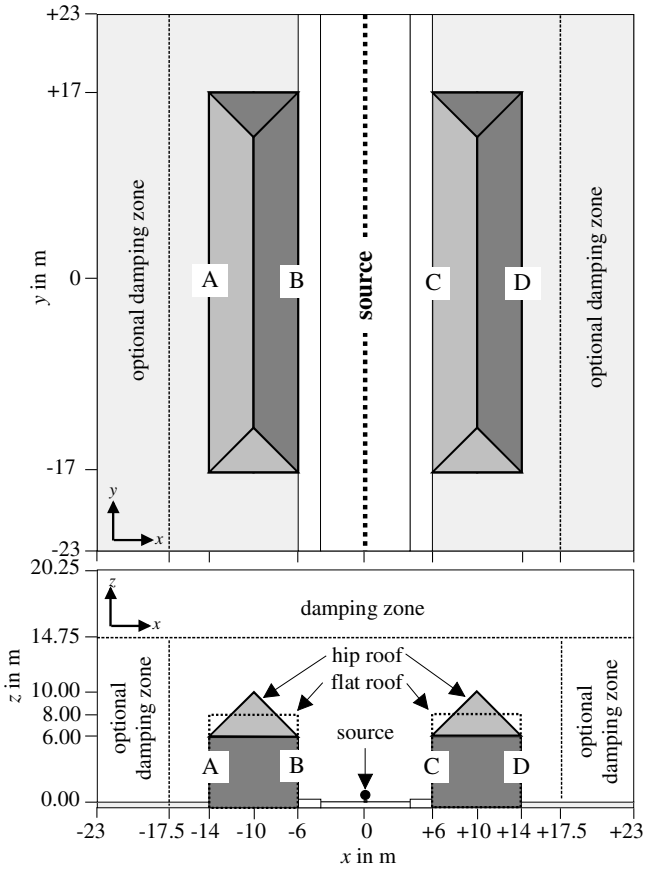

Fig. 1. Geometry of the numerical model domain, the source, and the buildings (top: plane view, bottom: vertical cross-section in the x–z plane). The street-parallel facades of the buildings are labelled by capital letters (A, B, C, D). In the numerical experiments with absorbing ground the light grey areas in the plane view are treated as grass-covered soil, while the white areas are treated as asphalt surfaces. The optional damping zones are effective in the case of absorbing boundaries in x-direction.

$L_z = 20.25$ m in the vertical direction ($n_z = 162$ intervals of $\Delta z = 0.125$ m). In addition, a ground layer of $L_{z,G} = 0.5$ m depth is resolved by $n_{z,G} = 20$ vertical grid intervals of $\Delta z_G = 0.025$ m. In the case of absorbing boundaries in x-direction, the damping zone should not be present too close to the buildings. Therefore, the width of the damping zone was limited to $d_0 = 5.5$ m such that $S_x = L_x - 2d_0 = 35$ m remains for the core domain. The horizontal damping zones commence at a distance of 3.5 m behind the back fronts of the buildings. The vertical damping zone begins at a height of $z = 14.25$ m, i.e., 6.25 m above the flat-roof buildings and 4.25 m above the ridge of the hip-roof buildings.

As an alternative to absorbing boundary conditions with damping zones in lateral directions, also cyclic (or periodic) boundary conditions were used. This is equivalent to the assumption that the geometry of the model domain (source, receiver, obstacles, etc.) repeats infinitely often in the respective direction. In the following study cyclic boundary conditions are always employed in y-direction. In combination with absorbing boundary conditions in x-direction and a line source along the y-axis, this corresponds to an effective geometrical configuration with an infinitely long street which is accompanied by rows of buildings on either side (Fig. 2(a)). Alternatively, cyclic boundary conditions are set both in x- and y-direction. This configuration corresponds to an extended town with infinitely long parallel streets (Fig. 2(b)). The effective extension in the x-direction depends on the chosen integration time, i.e., the longest possible propagation path. The simulated urban environments are of course highly idealised, but principle relationships between the geom-

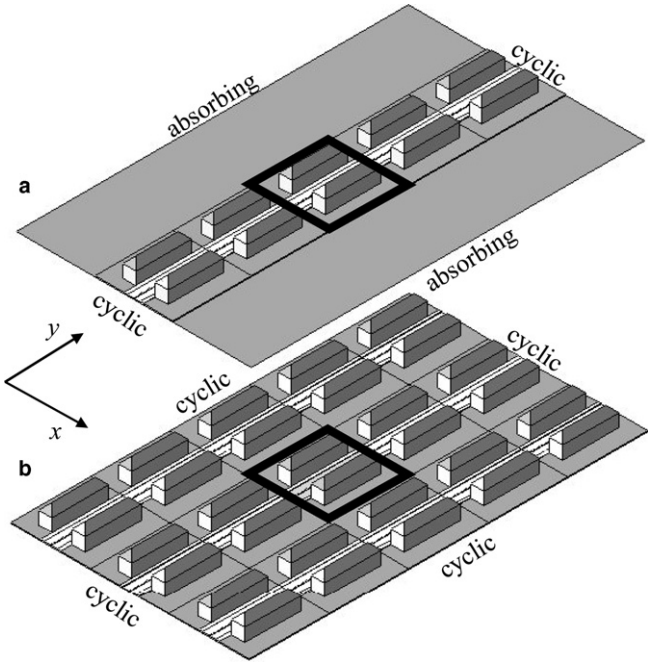

Fig. 2. Schematic view of the effective urban environments in the simulations with absorbing boundaries in x-direction and cyclic boundaries in y-direction (a) and cyclic boundaries in both (x- and y-) directions (b). The black frames indicate the actual model domain as shown in Fig. 1.

etry of buildings and noise emitting streets, ground properties, wind, turbulence and sound propagation can be studied.

Numerical requirements restrict the feasible frequency range. The respective relationships are described in Appendix A. Following Eq. (A.7) of the appendix with $c = 340$ m/s, $n_x = 368$, and $S_x = 35$ m, the limiting (maximum) frequency amounts to $f_{\lim} = 265$ Hz. Below this limit the consideration of a certain frequency range $f_{\min} < f_{\max} < f_{\lim}$ would be possible. According to Eq. (A.6) of the appendix, the following combinations of standard 1/3-octave band centre frequencies [6] could be covered by the simulations: (25, 31.5, 40, 50, 63, 80 Hz), (31.5, 40, 50, 63, 80, 100 Hz), (50, 63, 80, 100, 125 Hz), (63, 80, 100, 125, 160 Hz), (100, 125, 160, 200 Hz), or (200 and 250 Hz). Since low-frequency sound waves are of minor importance in urban noise and are almost not refracted by wind gradients, it was decided not to simulate multiple frequencies or broad banded sound (pulse source). Instead, the model is applied to a pure tone with the highest possible standard centre frequency, namely $f = 250$ Hz (wave length $\lambda = 1.36$ m with $c = 340$ m/s). The results of this study are of course not representative of the full spectrum of typical traffic noise. Moreover, the choice of one single frequency leads to interference patterns and requires specific evaluation methods (see Section 4.4).

4. Numerical experimentation

4.1. Accuracy tests

Three tests were performed to demonstrate the quality of the model in the context of the applications in this study.

In a first test the numerical accuracy and the effect of the damping zones was checked. The model was run in two dimensions (x–z-plane) for a homogeneous atmosphere above rigid ground. A constant source (250 Hz) was placed 0.5 above ground. Damping zones of $d_0 = 5.5$ m width were employed below the upper lid and in front of the right-hand lateral boundary. The resulting sound level distribution was compared with the analytical solution. Fig. 3 shows the difference in level (numerical minus analytical). Within the core of the domain the numerical result deviates by no more than 0.15 dB from the exact solution. With the beginning of the damping zones the numerical solution gradually drops to low levels and the difference becomes strongly negative. However, the deviation still remains below 1 dB up to a distance of 4 m from the absorbing boundaries.

A second test was performed to examine the influence of the top damping layer on the diffraction at the roof tops of buildings. Fig. 4 shows the difference between two simulations with and without a damping layer employed above $z \geqslant 15.25$ m. The simulation was terminated after 0.65 s such that sound waves which are reflected at the upper domain lid despite of the still existing impedance boundary condition cannot travel downward too far. Again differences larger than 1 dB occur only inside the damping layer while the diffraction at the roof top at $z = 10$ m, i.e., 5.25 m below the lower limit of the damping layer, is not affected by the damping layer. Below the damping layer the differences vary by only ± 0.1 dB due to numerical noise. This means that sound energy which has entered the layer above $z \geqslant 15.25$ m does not contribute to the sound energy in the shaded area behind the building.

In a third test the reflection at vertical walls was tested by evaluating the time behaviour of the energy-equivalent average sound level in the street 'canyon' between two 8 m high

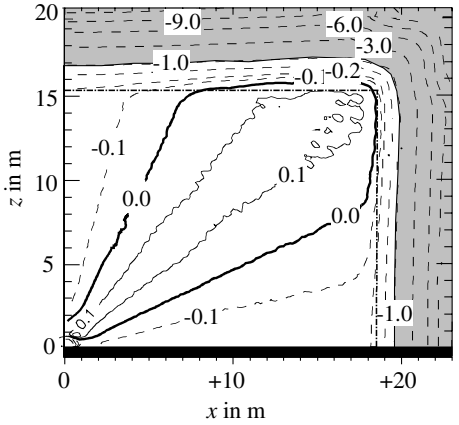

Fig. 3. Vertical cross-section showing the difference (in dB) of the numerically simulated sound level minus the analytical solution for a non-refracting atmosphere above rigid ground. The source (250 Hz) is placed at $x = 0$; $z = 0.5$ m. The numerical simulation considers damping zones for $x \geqslant +18.5$ m and $z \geqslant 15.25$ m (right and above the dash-dotted line). The grey shaded area indicates where the numerical solution deviates by more than 1 dB from the analytical one.

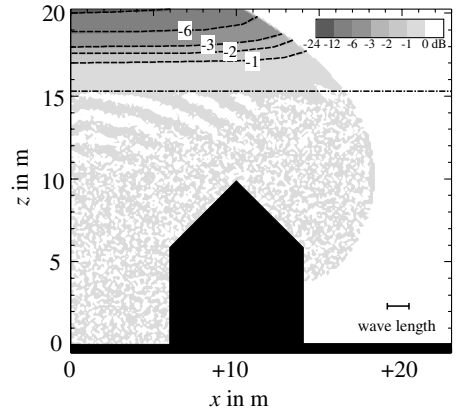

Fig. 4. Vertical cross-section showing the difference (in dB) of the sound level (after $t = 0.65$ s) 'with' minus 'without' a damping layer employed at the top boundary ($z \geqslant 15.25$ m; above the dash-dotted line) in the presence of a hip-roof building. The source ($f = 250$ Hz, $\lambda = 1.36$ m) is placed at $x = 0$; $z = 0.5$ m.

flat-roof buildings (Fig. 1). A calm atmosphere with uniform sound speed was assumed. A line source in the centre of the canyon was placed at $z = 0$ to avoid reflections at the ground surface. The walls of the buildings were considered as plane and rigid. Damping zones were installed at the lateral and top boundaries. After the source is turned on, the level rises until the emitted sound energy flux equals the one that leaves the street canyon at roof level. The sound waves are reflected back and forth at the opposing walls such that an increasing number of reflections contribute to the average level within the canyon. After 0.4 s the sound source was turned off. The average sound level does not drop immediately, but ceases gradually because of reverberation. The decline of the level is determined by the travel time of the remaining sound waves which are still reflected between

the walls. The numerically calculated time evolution of the energy-equivalent average sound level in the street canyon was compared with the analytical solution which superimposes the sound waves of all contributing propagation paths (direct ray and multiply reflected rays). The analytical solution is simply the addition of the complex sound pressure associated with a successively increasing number of straight rays emerging from a series of geometrically determined mirror sources locations.

Fig. 5 shows the time behaviour of both solutions. The increase of the level after the source is switched on is almost identical. During the equilibrium phase ($0.1 \leqslant t \leqslant 0.4$ s) the levels are constant. After the source is switched off the solutions of the decay equal only within the first 1.5 s ($0.4 \leqslant t \leqslant 0.55$ s). Then the numerical solution decreases faster. It is assumed that this is caused by numerical diffusion, i.e., inaccuracies of the numerical scheme. Fig. 4 also indicates the number of reflections involved. Until $t = 0.4$ s up to 11 reflections are involved. This corresponds to reflected propagation paths of up to 138 m length while the longest direct ray within the cross-section of the street canyon merely comes up to 10 m.

4.2. Experimental setup

Eighteen different numerical experiments were performed (Table 1). Two of them (E100 and E200) serve as reference without buildings and wind. In all cases a coherent

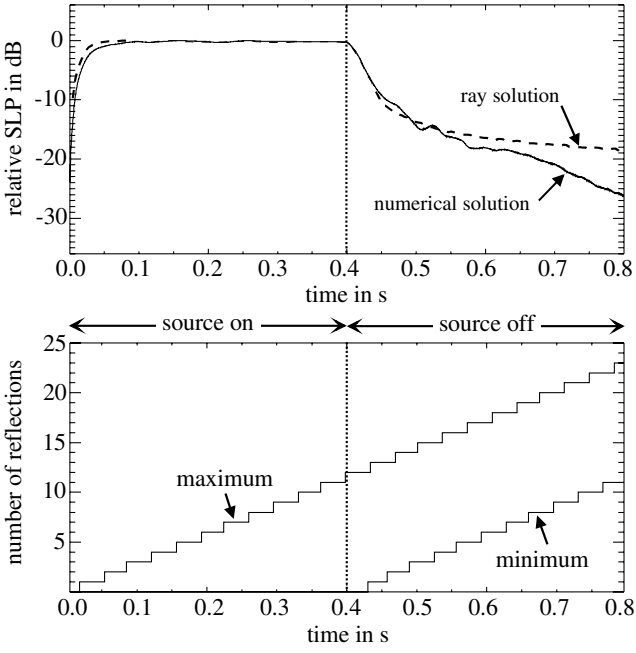

Fig. 5. Time evolution of the mean energy-equivalent sound level (relative to equilibrium) in a 12 m wide and 6 m high street canyon. The source is placed at ground in the centre of the canyon and emits steady sound of 250 Hz during the first 0.4 s. The solid curve in the upper panel shows the numerical solution while the broken line indicates the analytical solution. The lower panel shows the minimum and maximum number of reflections at the side walls of the canyon.

Table 1
Numerical experiments

Experiment	Boundaries in x-direction	Building	Roof type	Ground type	Wind	Turbulence
E100	Absorbing	No	No	Rigid	No	No
E110	Absorbing	Yes	Flat	Rigid	No	No
E111	Absorbing	Yes	Flat	Rigid	Yes	No
E112	Absorbing	Yes	Flat	Absorbing	Yes	No
E113	Absorbing	Yes	Flat	Absorbing	Yes	Yes
E120	Absorbing	Yes	Hip	Rigid	No	No
E121	Absorbing	Yes	Hip	Rigid	Yes	No
E122	Absorbing	Yes	Hip	Absorbing	Yes	No
E123	Absorbing	Yes	Hip	Absorbing	Yes	Yes
E200	Cyclic	No	No	Rigid	No	No
E210	Cyclic	Yes	Flat	Rigid	No	No
E211	Cyclic	Yes	Flat	Rigid	Yes	No
E212	Cyclic	Yes	Flat	Absorbing	Yes	No
E213	Cyclic	Yes	Flat	Absorbing	Yes	Yes
E220	Cyclic	Yes	Hip	Rigid	No	No
E221	Cyclic	Yes	Hip	Rigid	Yes	No
E222	Cyclic	Yes	Hip	Absorbing	Yes	No
E223	Cyclic	Yes	Hip	Absorbing	Yes	Yes

line source was placed in the centre of the street and 0.5 m above ground ($x = 0$; $z = 0.5$ m). At the grid points of the source the time behaviour of the sound pressure $p''(t)$ was prescribed as a constant harmonic oscillation with a frequency of $f = 250$ Hz and an amplitude of $\hat{p} = 1$ Pa. The experimental setup was designed to study the combined effects of two roof shapes and wind on the impact of street noise at the back ('quiet') facades of the buildings in two idealised urban environments. Simulations were performed both for flat-roof buildings and hip-roof buildings without roof overhangs. For simplicity, the surfaces of the buildings were always considered as plane, rigid and non-diffusive. By the choice of absorbing or cyclic boundaries in x-direction, two different urban environments were considered (a single infinitely long street or parallel infinitely long streets; see Fig. 2). In some experiments wind (with and without turbulence) or absorbing ground was taken into account (see Section 4.3). The numerical experiments are summarised in Table 1.

4.3. Ground, wind field, turbulence

Basic sound propagation simulations were performed for rigid ground surfaces. Alternative numerical experiments consider absorbing ground where the parameters in Eq. (4) were set to values typical of asphalt (blank area in Fig. 1; $\sigma = 60$ kPa s m^{-2},$\Omega = 0.28$, $c_s = 33.9$) and grass (grey area in Fig. 1; $\sigma = 50$ kPa s m^{-2}, $\Omega = 0.20$, $c_s = 0.1$).

A part of the numerical experiments considers a wind field which is distorted by the buildings. The wind field is calculated with the help of a three-dimensional numerical flow model (for a description, see [1] or [7]). Given an undisturbed background wind profile, the model provides the spatial distribution of the steady-state mean wind flow over and around the buildings and the corresponding spatial distribution of the turbulent kinetic energy (TKE), i.e., the mean kinetic energy of the turbulent wind fluctuations superimposed to the mean flow as a measure of the local strength of turbulence.

A logarithmic wind profile

$$V(z) = \frac{u_*}{k} \ln\left(1 + \frac{z}{z_0}\right) \tag{5}$$

was used to initialise the model. It defines the undistorted meteorological background situation. The roughness length and the friction velocity were set to $z_0 = 0.1$ m and $u_* = 0.6932$ m/s, respectively. With the von Karman constant $k = 0.4$ this leads to a rather high background wind speed of 8 m/s at a height $z = 10$ m above ground. The direction of the background flow (30° with respect to the x-axis) was specified to ensure asymmetry in the wind field with respect to all space axes. Since the geometry of ground types and buildings is symmetric with respect to the x- and y-axis, all asymmetries in the resulting noise fields can be attributed to the wind field. The flow model was applied to the flat-roof and hip-roof buildings. For hip-roof buildings and cyclic boundary conditions in x- and y-direction the resulting mean wind flow is shown in Fig. 6. The wind flow is strongly influenced by the buildings. Large vortices with horizontal axes form between the buildings with a return flow near the ground. Smaller vortices with vertical axes are found in the wake of the downwind end of the houses. Fig. 7 shows the simulated profiles of the x-component of the wind and the turbulent kinetic energy above the centre of the street canyon and above the centre of the roof of the downwind building. In the case of the hip-roof building the wind speed is smaller (because the hip-roof buildings extends to a larger height), but the vertical gradient immediately above the roof ridge is higher. The strong vertical gradient above the hip roofs causes a stronger turbulence than for flat-roof buildings.

In another set of simulations, turbulence was taken into account. Three-dimensional random fields of turbulent wind eddies were numerically generated and superimposed to the mean wind field in intervals of $\tau = 2/f$ (twice the period) such that the sound propagates through a varying wind field. The mean amplitude of the turbulent flow components was chosen such that it locally corresponds to the simulated TKE. The diameter of the sphere-like turbulent eddies is restricted to a range between $4\Delta z = 0.5$ m and $0.5L_z - 4\Delta z = 9.875$ m. Hence, only turbulence due to shear flow near ground and buildings is considered. Larger, externally (in the atmospheric boundary-layer above the model domain) generated turbulent eddies remain disregarded. Details of the numerical turbulence generator are published in [7].

4.4. Time integration and evaluation

The time integration of the model equations is stopped at the time $t_e = 0.4$ s after initialisation. In the case of absorbing boundaries in x- and z-direction the sound energy content inside the model domain has already levelled off at this time, i.e., the sound energy emission at the source equals the sound energy absorption at the absorbing domain boundaries. In the case of cyclic boundaries in x- and y-direction, the termination time of $t_e = 0.4$ s ensures that propagation paths of up to 136 m length are considered. This corresponds to almost three times the width of the model domain, i.e., the actual model domain is affected by the sound of the centre street and that of at least two parallel streets on either side.

If turbulence is considered, the mean flow field is superimposed by pre-calculated fields of turbulent random wind components after the whole domain was filled by sound, i.e., during

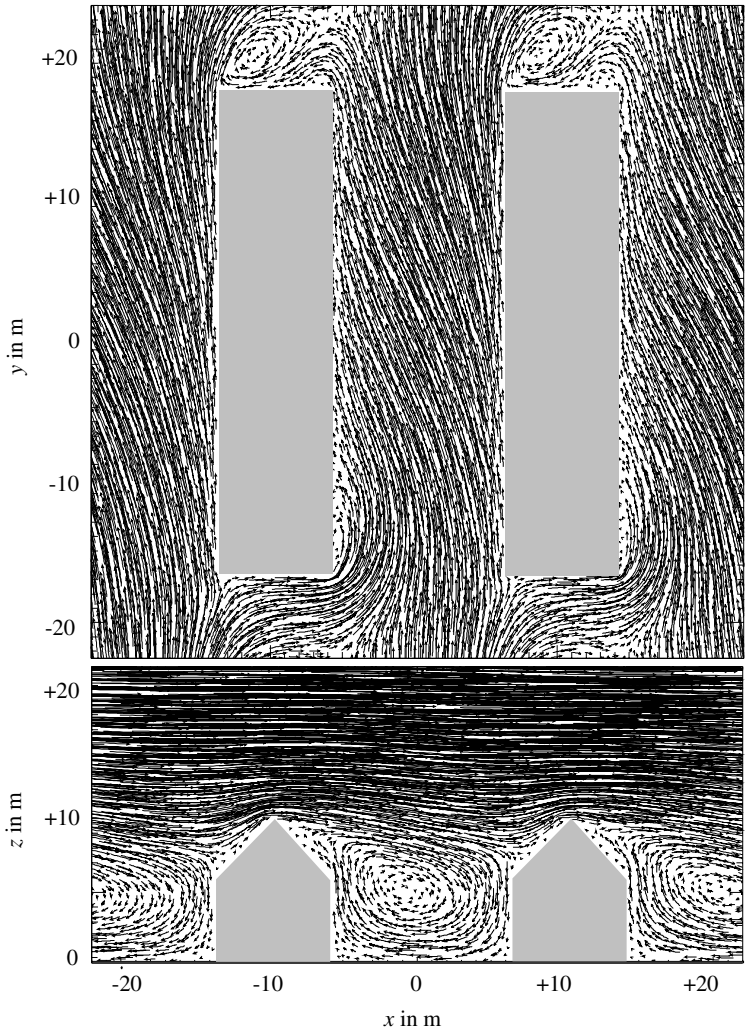

Fig. 6. Simulated wind field (top: x–y-plane at $z = 1.5$ m above ground; bottom: x–z-plane at $y = 0$) in the presence of hip-roof buildings. The arrows correspond to wind traces of 0.6 s duration.

the time period $t_s \leqslant t \leqslant t_e$ with $t_s = 0.2$ s and $t_e = 0.4$ s. The turbulent wind patterns are exchanged in intervals of two periods ($2\tau = 2f^{-1} = 0.008$ s). In total, $0.5(t_e - t_s)f = 25$ different realisations of turbulence are encountered by the sound waves during their travel time.

The model output consists in the 3D field of the effective sound pressure amplitude

$$\hat{p}(x,y,z) = \left(\frac{1}{t_2 - t_1}\int_{t_1}^{t_2} p^2(x,y,z,t)\,\mathrm{d}t\right)^{1/2} \tag{6}$$

with $t_1 = t_e - 2\tau$ and $t_2 = t_e$ in the case of no turbulence and $t_1 = t_s$ and $t_2 = t_e$ in the case of turbulence. In the following, the effective sound pressure amplitude is expressed by the sound pressure level relative to $p_0 = 2 \times 10^{-5}$ Pa.

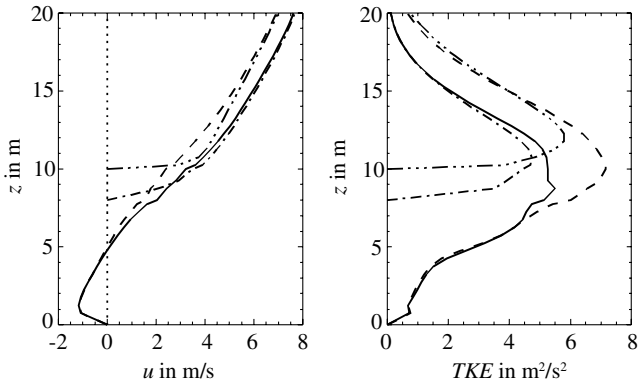

Fig. 7. Simulated vertical profiles of the x-component of the wind u (left panel) and the TKE (right panel). The profiles refer to the centre of the street ($x = 0, y = 0$; solid curves for flat-roof buildings and dashed curves for hip-roof buildings) and the roof of the right-hand buildings ($x = +10$ m, $y = 0$; dash-dot curves for flat-roof buildings and dash-dot-dot-dot curves for hip-roof buildings).

The use of a single frequency (250 Hz) noise source has the consequence that the resulting sound field exhibits rather complex interference patterns. These patters would already change its appearance substantially if the source is only a little displaced. The exact position of these interference patterns is therefore irrelevant. To enable a better interpretation of sound level fields the results are treated in two different manners. As a first method the sound pressure amplitudes $\hat{p}(x, y, z)$ are smoothed by applying a moving energy-equivalent average within cubes of an edge length of 22 grid cells (2.75 m), i.e., approximately twice the wave length. All small-scale interference patters are removed by this method. As a second method the energy-equivalent mean-values of the sound level over the full extension of the facades are calculated. In addition, the frequency distributions of the sound level (based on non-smoothed pressure amplitudes) are evaluated.

Despite the above described evaluation method, the findings from the 250 Hz results cannot be simply transferred to other frequencies since diffraction, scattering and reflection (at absorbing ground) depends on the wave length. It can be expected that many effects are more pronounced for frequencies higher than the here used 250 Hz.

5. Results

The results of the model experiments are presented in the following manner. The pure shading effect of the buildings (flat and hip roof) is shown in Fig. 8 in a vertical cross-section at $y = 0$. The basic wind effect on the noise level at the back fronts of the buildings is illustrated in Fig. 9, again for both roof types. Eventually, all effects (wind, roof shape, ground property, turbulence) are compared in Figs. 11–13 with the help of frequency distributions and energy-equivalent averages of the sound levels over the facade areas.

The pure shading effect by the building for a non-refraction atmosphere is illustrated in Fig. 8 for flat- and hip-roof buildings. The vertical cross-section refers to the x–z-plane at $y = 0$ and shows the sound pressure level relative to the reference (flat roof: E110-E100; hip roof: E120-E100). The sound levels are based on smoothed pressure amplitudes (see Section 4.4). A homogeneous resting atmosphere and rigid ground are assumed. Only

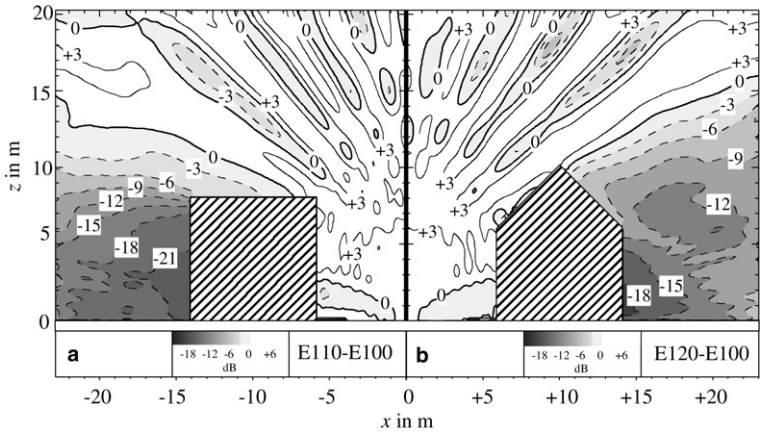

Fig. 8. Shading effect (in dB) of the buildings in a non-refracting atmosphere. 250 Hz sound waves are emitted at $x = 0, z = 0.5$ m. (a) Flat-roof buildings (experiment E110-E100), (b) hip-roof buildings (experiment E120-E100).

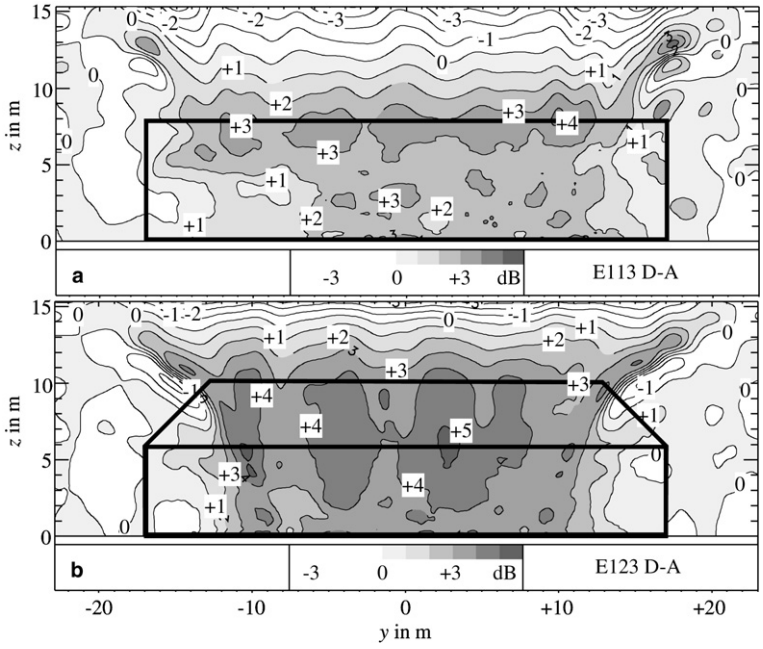

Fig. 9. Wind effect (in dB) in the case of the experiments with absorbing ground, turbulence and absorbing boundaries in x-direction ((a) E113 for flat-roof building, (b) E123 for hip-roof building). The contours show the difference of the simulated sound pressure levels between the y–z-plane at $x = +14$ m (downwind facade D) and the y–z-plane at $x = -14$ m (upwind facade A).

one part of the cross-section is shown for each roof-type because the results are symmetric with respect to $x = 0$. Inside the street canyon the sound level is increased by about 3 dB due to multiple reflections between the street facades B and C. At the back facades A and

D the sound level is significantly reduced by the shading effect of the buildings. However, the levels differ by about 4 dB between the two roof types with the higher value on the rear side of the hip-roof building. This means that the hip-roof building, although it has the same cross-cut area and is even higher than the flat-roof building, is less effective in protecting the back facades from the noise of the street. The main reason is the difference in the propagation paths of the diffracted sound. In the case of the flat-roof building a first diffraction (by an angle of 90°) occurs already at the street-side roof edge while due to the chosen geometry of the hip-roof building the first diffraction only occurs on top of the roof ridge (again by an angle of 90°). The second diffraction edge is located 8 m behind the first one in the case of the flat roof, but only 5.67 m in the case of the hip roof. Moreover, the second diffraction edge of the flat-roof building bends again by 90°, while that of the hip-roof building bends by merely 45°. The slightly smaller volume of the hip-roof buildings and their different aerodynamic properties could also contribute to the reduced efficiency in sheltering the sound.

If the asymmetric wind field (Section 4.3) is considered, the sound waves which arrive at facades A and D are differently refracted. Towards facade A the sound waves propagate in upwind direction and are thus upward refracted. On the contrary, they propagate downwind and are downward refracted on their way to facade D. Therefore, the noise level at facade D is expected to be higher than that at facade A. In addition, the oblique flow also leads to asymmetries in the noise impact with respect to $y = 0$. The asymmetries in the sound field are shown in Fig. 9 for the experiments with absorbing ground and turbulence (flat roof: E113, hip roof: E123). It shows the difference in the sound levels (based on smoothed sound pressure amplitudes) between the facades A ($x = -14$ m) and D ($x = +14$ m). At the downwind facade D the sound level is by up to 5 dB higher than at the upwind facade A. The wind effect is stronger in the case of the hip-roof building, presumably because the vertical wind speed gradients above the hip-roof ridge is stronger than above the flat roof (see Fig. 7). Downward refraction is thus intensified by the hip roofs. The largest differences between the facades were simulated in the level of the roof (flat roof), respectively, the roof edge (hip roof). The asymmetry with respect to $y = 0$ is caused by the wind component parallel to the buildings and the horizontal wind speed gradients. They lead to horizontal refraction of the sound which is diffracted around the vertical edges of the buildings.

In the following, the bulk effect of the considered influences (wind, roof type, ground, turbulence, urban environment) at the facades is discussed. For each model experiment the energy-equivalent mean sound level was calculated over the full extension of each longitudinal facade (34×8 m^2 for the flat-roof buildings, 34×6 m^2 for the hip-roof buildings). In addition, the frequency distributions of the sound levels at the facades were determined. These distributions refer to the sound levels which are based on the non-smoothed simulated sound pressure amplitudes.

In the following we discuss not only the effect of the roof types, but also the consequence of cyclic boundaries in x-direction. Fig. 10 shows the geometry of the effective model domain in the latter case. At the back facades A of row C1 of buildings sound can arrive by three ways: (1) sound is emitted on street C and crosses the buildings of row C1 by diffraction, (2) sound is emitted on street L and crosses the buildings of row L2 by diffraction, (3) sound is emitted on street C, crosses the buildings of row C1 by diffraction, and is reflected at facade D of row L2 of buildings. The same applies analogously to facade D of row C2. The minimum path length between the source and the base of

facade A of row C1 is 26 m for (1), 37.7 m for (2) and 54.8 m for (3). These figures refer to flat-roof buildings. They increase by 3.3 m in the case of hip-roof buildings. Since the simulation time of $t_e = 0.4$ s permits path lengths of up to 136 m also multiple reflections between facade A of row C1 and facade D of row L2 and contributions from further parallel streets (not shown in Fig. 10) are included in the simulations. From the path lengths it can be assumed that path (1) contributes most to the sound level at facade A of row C1, while (2) contributes less and (3) least. Of course the relative contribution also depends on the number of diffraction edges and the respective diffraction angles which are encountered.

The situation with buildings, but without wind, is illustrated in Fig. 11. Because of the symmetry with respect to $x = 0$, the levels at the back facades A and D (of street C) are identical. As discussed in Figs. 8 and 9, the mean sound level at the back facades of the hip-roof buildings in the case of absorbing boundaries in x-direction (E120) is by 2.1 dB higher than that of the flat-roof buildings (E110). Accordingly, the frequency distribution of levels is shifted to higher levels. In the case of cyclic boundaries (flat roof: E210 and hip roof: E220) the back facades additionally benefit from sound emitted by the parallel streets L and R (see Fig. 10) and further parallel streets. They also benefit from sound reflected at the back facades of the buildings along the parallel streets. This leads to a higher sound level (by 5–7 dB in average) while the difference between flat-roof and hip-roof buildings vanishes.

Fig. 12 presents the numerical results for the model simulations with absorbing boundaries in x-direction. This condition in combination with a line source along the y-axis corresponds to the assumption of a single infinitely long noise-emitting street with buildings on either side. The left and right column of Fig. 12 show the result for flat-roof and hip-roof buildings, respectively. All experiments consider wind. The ground was assumed to be rigid in the experiments E111 (flat roof) and E121 (hip roof) and absorbing in the experiments E112 (flat roof) and E122 (hip roof). Turbulent wind and absorbing ground was assumed in the experiments E113 (flat roof) and E123 (hip roof). The frequency distributions are displayed for the back fronts A and D only, while the spatial energy-equivalent average sound levels are indicated as numbers for all facades. The source is identical for all experiments such that the absolute levels can be compared to each other.

In general, the noise level is higher on the back facades of the 10 m high hip roof than on the back facades of the 8 m high flat-roof buildings. Hence, the existence of a wind does

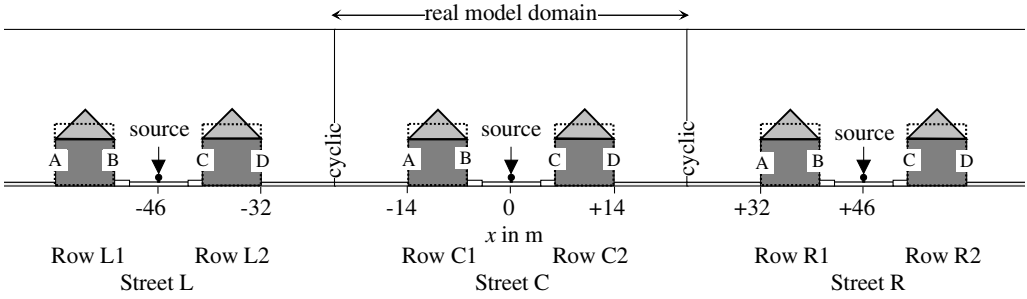

Fig. 10. Vertical cross-section (x–z-plane at $y = 0$) of the effective domain of the experiments with cyclic boundaries in x-direction. The streets and the rows of buildings are labelled.

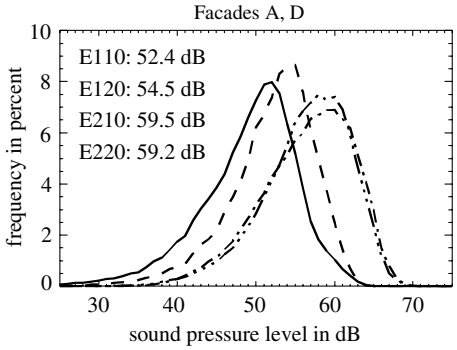

Fig. 11. Frequency distribution of sound levels at the facades A and D for the simulations without wind and above rigid ground. Solid: E110 (flat roof, absorbing boundary in x-direction), broken: E120 (hip roof, absorbing boundary in x-direction), dash-dots: E210 (flat roof, cyclic boundary in x-direction), dash-dot-dot-dots: E220 (hip roof, cyclic boundary in x-direction). The energy-equivalent mean levels over the extension of the facades are indicated in the upper-left corner of the panels.

not change the finding that was achieved for the simulations without wind (E110, E120; see discussion of Fig. 8). The average noise level of the downwind facade D is generally higher than that of the upwind facade A. Absorbing ground lowers the average levels by 0.7–1.0 dB (street fronts B and D) and by 1.3–1.5 dB (back fronts A and D). Introducing turbulence in addition to absorbing ground hardly changes the average levels further. The only effect induced by turbulence is a slight 'filling' of the interference minima which is caused by the loss of coherence.

A rather different picture is obtained, if cyclic boundaries are set in x-direction (Fig. 13) and sound from parallel streets is additionally involved. Now the downwind facade D does no longer show higher sound levels. On the contrary, the level at the upwind facade A is by 0.8 to 1.2 dB louder than that at facade D. The reason is the fact that facade A is downwind with respect to noise originating from the parallel street L while it is upwind with respect to noise originating from street R. This is sketched in Fig. 14. Because of the relatively long propagation paths (from street L to facades A of buildings C1 and from street R to facades D of buildings C2) the refraction is more effective than for the propagation from street C to the facades A and D of the adjacent buildings C1 and C2. This leads to an overcompensation of the wind effect which was found for the simulations with absorbing boundaries in x-direction. Assuming absorbing instead of rigid ground lowers the mean levels at the facades by -1.6 dB (facade A, flat roof), -2.0 dB (facades D, flat roof), -2.5 dB (facades A, hip roof), and -2.3 dB (facades D, hip roof). The consideration of the building-induced turbulence further lowers the sound level, especially in the case of flat-roof buildings (-1.2 dB at facades A and -0.9 dB at facades D). The decrease in level due to turbulence can be explained by the destruction of the sharp vertical gradients above the buildings which reduces the downward refraction of sound (between the roof of buildings L2 and facades A as well as between the roof of buildings C2 and facades D). Because of the longer propagation paths (relative to the experiments with a single street) the effect of turbulence is this time stronger. This does not only apply to the mean levels, but also to the frequency distributions which are now narrower than in the cases without turbulence.

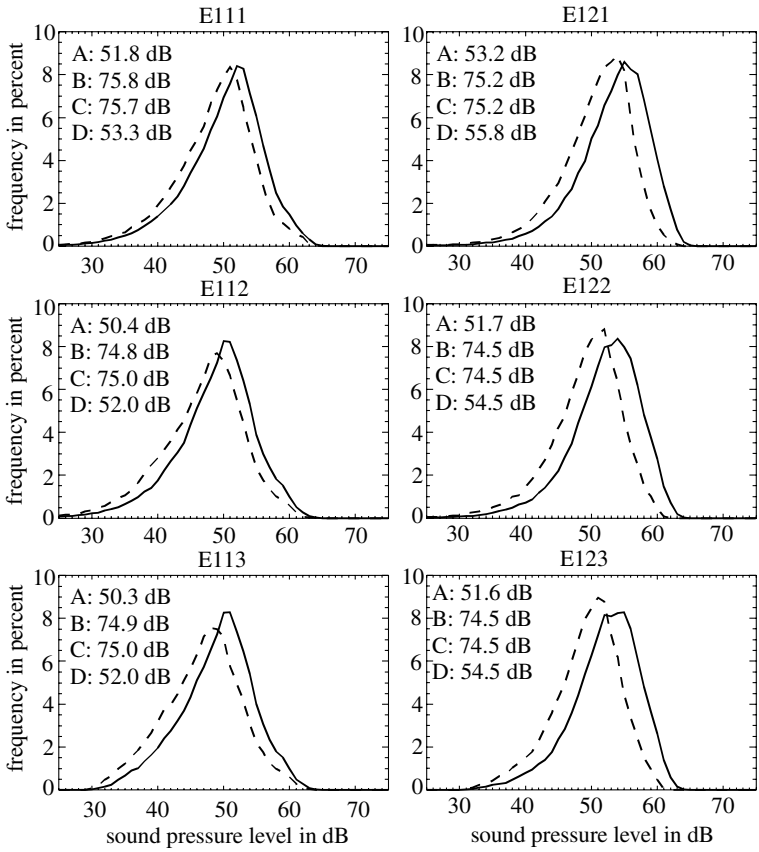

Fig. 12. Frequency distribution of simulated sound levels at the facades A (dashed) and D (solid) for flat-roof buildings (left column) and hip-roof buildings (right column). The energy-equivalent mean levels over the extension of the facades A, B, C, D are indicated in the upper-left corner of the panels. The experiment identifiers (see Table 1) are indicated at the top of the panels. Absorbing boundaries are set in x-direction.

6. Discussion and conclusions

Numerical time-domain finite-difference LE models can be applied in three dimensions to urban situations with isolated buildings and asymmetric wind fields. However, the memory capacity of available computers is a very limiting factor for simulations with this type of models. Consequently, the spatial resolution, the domain size and thus the possible dimension of buildings is confined. Numerical requirements furthermore restrict the frequency range of simulated sound waves and do not admit high frequencies unless the spatial resolution is sufficiently high. The usefulness of LE models for the solution of typical traffic noise problems encountered in practice is therefore still rather limited. If the performance of computers continues to increase like in the past however, the application of three-dimensional LE-models to common urban noise problems will become more and more feasible.

The use of cyclic (instead of absorbing) boundary conditions at two opposing or all four lateral limits of a rectangular model domain enlarges the effective model domain in an

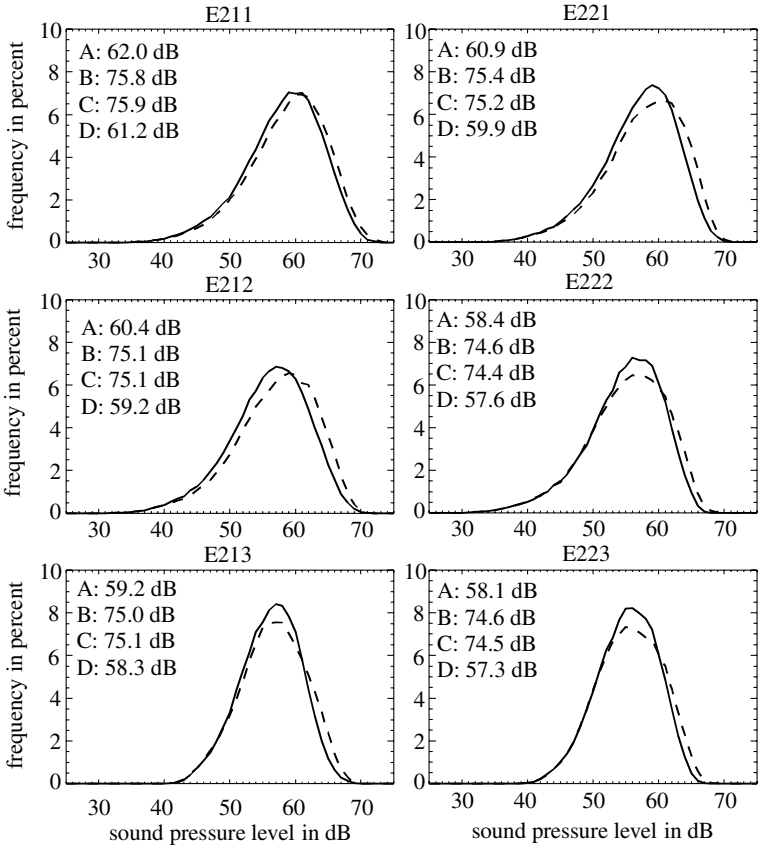

Fig. 13. Same as Fig. 12, but for cyclic boundaries in x-direction.

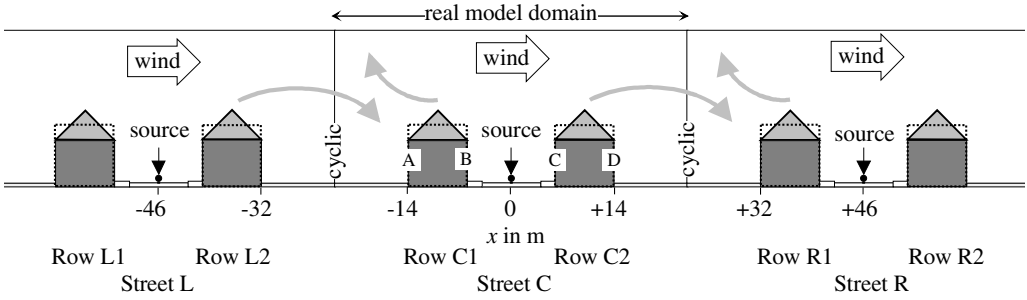

Fig. 14. Vertical cross-section (x–z-plane at $y = 0$) of the effective domain of the experiments with cyclic boundaries in x-direction. The direction of the x-component of the mean wind above the roof-edge level is indicated by the arrow "wind". The light grey arrows symbolise the direction of sound refraction (downward or upward) due to the mean wind. The streets and the rows of buildings are labelled.

idealised manner but does not allow for real situations. Despite these limitations, the model was used for basic and rather idealised studies of the effects of roof-types, ground properties, wind flow, and turbulence on the propagation of street noise to the back fronts

of the considered buildings. Although the model was applied to only two types of buildings (flat and hip roof) in this study, the model resolution would principally allow to resolve various building shapes (including roof overhangs, ledges and balconies) and to study their effects.

The roof type (flat or hip) turned out to have a major effect to the sound impact on the back fronts because it determines the length of the propagation path across a building and the number and angle of diffraction edges. For buildings with identical cross-cut areas flat roofs are more effective in preventing the back fronts from street noise. On the other hand, hip roofs enhance the wind effect such that the shading effect is reduced at the back facade of the downwind building more strongly than for flat roofs. The assumed oblique air flow leads to asymmetries of the noise impact in the street parallel direction. Absorbing (instead of rigid) ground only reduces the sound level, but does not change the relative effects. Turbulence did not lead to a significant modification of the results, probably because the propagation paths are too short. The above findings are valid if absorbing conditions are employed at the lateral domain boundaries parallel to the street. This corresponds to a geometry with one single (noise emitting) street and building on either side of this street. Consequently, the back fronts of the buildings are only exposed to noise of this street.

Different findings are obtained if cyclic conditions are applied to all lateral boundaries. This configuration is equivalent to an extended urban area with parallel (noise emitting) streets. The street-parallel facades are now exposed to noise from more than one street. The back front of a building receives diffracted sound from the own street but it also receives sound from the parallel street the front is facing to. A consequence of this configuration is a decrease of the wind effect, i.e., upwind and downwind facades do almost not differ anymore with respect to noise impact.

The findings from the numerical experiments are only valid for a 250 Hz tone as it was always prescribed here. For high frequency sound (short wave lengths) it can be expected that the boundaries of acoustical shadows are sharper and the effect of refraction is stronger.

Therefore, the investigated effects are presumably more pronounced for frequencies higher than 250 Hz and less pronounced for frequencies lower than 250 Hz.

Acknowledgements

This study was motivated by cooperations within the European project HARMONOISE which was funded by the European Commission under Contract IST-2000-28419. The author thanks his wife Elisabeth Hagenmeyer for CAD drawings.

Appendix A. Computational limitations

Three-dimensional LE models are rather pretentious with respect to CPU time and memory and their application is therefore limited due to the available resources. The maximum size of the 3D model domain and the spatial resolution is determined by numerical requirements and the maximum available core memory capacity of the computer. In the following, the relationship between domain extension, number of grid intervals, spatial resolution and frequency range is illustratively derived for the x-direction.

The horizontal extension of the model domain in direction x is given by

$$L_x = n_x \Delta x = S_x + 2d_0, \tag{A.1}$$

where n_x and Δx are the number and the length of the grid intervals, respectively. S_x is the usable domain extension, i.e., the full domain extension minus twice the width d_0 of the damping zones that are employed at both lateral boundaries to suppress unwanted numerical reflections in the case of absorbing boundaries.

The numerical scheme requires that a sound wave has to be resolved by at least 10 grid intervals. The grid interval Δx therefore depends on the minimum wave length $\lambda_{\min}$ or the maximum frequency $f_{\max}$

$$\Delta x \leqslant \frac{1}{10}\lambda_{\min} = \frac{1}{10}\frac{c}{f_{\max}}, \tag{A.2}$$

where c is the speed of sound relative to the air.

As mentioned in Section 2 the minimum width of the damping zone d_0 depends on the maximum wave length or the minimum frequency:

$$d_0 \geqslant 4\lambda_{\max} = 4\frac{c}{f_{\min}}. \tag{A.3}$$

Hence, the possible frequency range is bounded according to

$$\frac{4c}{d_0} \leqslant f \leqslant \frac{c}{10\Delta x}. \tag{A.4}$$

The maximum core memory capacity of the computer determines the maximum number of grid meshes $N_{\max}$:

$$n_x \cdot n_y \cdot n_z = N \leqslant N_{\max}. \tag{A.5}$$

Normally, the maximum number of grid cells $N_{\max}$ and thus the number of intervals in x-direction n_x is controlled by the storage capacity of the computer while the minimum extension of the usable model domain S_x is fixed according to the maximum source–receiver distance. In this case the possible frequency range follows from Eqs. (A.1)–(A.3):

$$f_{\max} = \frac{n_x c}{80 c f_{\min}^{-1} + 10 S_x}. \tag{A.6}$$

In addition, the condition $f_{\min} \leqslant f_{\max}$ implies that a limiting frequency $f_{\lim}$ exists with

$$f_{\max} \leqslant f_{\lim} = \frac{(n_x - 80)c}{10 S_x}. \tag{A.7}$$

Eqs. (A.6) and (A.7) mean that only a small band of frequencies is permitted unless the number of grid intervals is very large or the usable domain extension is small.

References

[1] Blumrich R, Heimann D. A linearized Eulerian sound propagation model for studies of complex meteorological effects. J Acoust Soc Am 2002;112:446–55.

[2] Blumrich R, Heimann D. Numerical estimation of atmospheric approximation effects in outdoor sound propagation modelling. Acta Acustica 2004;90:24–37.

[3] Botteldooren D. Acoustical finite-difference time-domain simulation in a quasi-cartesian grid. J Acoust Soc Am 1994;95:2313–9.

[4] Botteldooren D. Time-domain simulation of the influence of close barriers on sound propagation to the environment. J Acoust Soc Am 1997;101:1278–85.
[5] Brown EF, Dennis EB, Henry J, Pendray FE, editors. City noises. New York: Academic Press; 1930.
[6] ISO 9613-2. Attenuation of sound during propagation outdoors – Part 2: general methods of calculation. Obtainable from the International Organization for Standardization. Available from: http://www.iso.org.
[7] Heimann D, Blumrich R. Time-domain simulations of sound propagation through screen-induced turbulence. Appl Acoust 2004;65:561–82.
[8] Heutschi K. A simple method to evaluate the increase of traffic noise emission level due to buildings for a long straight street. Appl Acoust 1995;44:259–74.
[9] Iu KK, Li KM. The propagation of sound in narrow street canyons. J Acoust Soc Am 2002;112:537–50.
[10] Kang J. Sound propagation in street canyons: comparison between diffusely and geometrically reflecting boundaries. J Acoust Soc Am 2000;107:1394–404.
[11] Kang J. Numerical modelling of the sound fields in a urban street with diffusely reflecting boundaries. J Sound Vibr 2002;258:793–813.
[12] Kuttruff H. A mathematical model for noise propagation between buildings. J Sound Vibr 1982;85:115–28.
[13] Le Pollès T, Picaut J, Bérengier M, Bardos C. Sound field modeling in a street canyon with partially diffusely reflecting boundaries by the transport theory. J Acoust Soc Am 2004;116:2969–83.
[14] Makarewicz R. Traffic noise in a built-up area. Appl Acoust 1991;34:37–50.
[15] Oldham DJ, Radwan MM. Sound propagation in city streets. Build Acoust 1994;1:65–87.
[16] Picaut J, Simon L, Hardy J. Sound field modeling in streets with a diffusion equation. J Acoust Soc Am 1999;106:2638–45.
[17] Picaut J. Numerical modeling of urban sound fields by a diffusion process. Appl Acoust 2002;63:965–91.
[18] Salomons EM, Blumrich R, Heimann D. Eulerian time-domain model for sound propagation over a finite-impedance ground surface. Acta Acustica 2002;88:483–92.
[19] Van Renterghem T. The finite-difference time-domain method for simulation of sound propagation in a moving medium. PhD thesis, University of Gent, Belgium; 2003.
[20] Walerian E, Janczur R, Czechowicz M. Sound level forecasting for city-centers. Part 1: sound level due to a road within an urban canyon. Appl Acoust 2001;62:359–80.